chemosensors

Article

Radical TTM-DMODPA for Ascorbic Acid Non-Catalytic Visual Detection

Qingmei Zhong, Huixiang Zong, Xiaohui Xie, Xiaomei Rong and Chuan Yan *

Hunan Engineering Research Center for Monitoring and Treatment of Heavy Metals Pollution in the Upper Reaches of Xiangjiang River, College of Chemistry and Materials Science, Hengyang Normal University, Hengyang 421008, China

* Correspondence: chuanyan2019@163.com

Abstract

Ascorbic acid (AA) plays a multidimensional role in human physiological and pathological processes, and the detection of its urinary concentration facilitates the diagnosis of metabolic or kidney diseases. Visual detection exhibits minimal reliance on instrumentation and is suitable for on-site analysis in routine settings. Current visual colorimetric detection methods typically rely on enzymatic or nanozyme-based catalysis. Organic neutral radicals bearing unpaired electrons represent a class of materials exhibiting intrinsic responsiveness to redox stimuli. The tris (2,4,6-trichlorophenyl) methyl (TTM) radical has attracted widespread attention for its adjustable optical properties and sensitive response to external redox stimuli. We synthesized a novel radical TTM-DMODPA and applied it for non-catalytic colorimetric detection of AA. It not only enables quantitative AA measurement via UV-vis spectroscopy (linear range: 1.25–75 μmol/L, LOD: 0.288 μmol/L) but also facilitates instrument-free visual detection using smartphone cameras (linear range: 0–65 μmol/L, LOD: 1.46 μmol/L). This method demonstrated satisfactory performance in the measurement of AA in actual urine samples. Recovery rates ranged from 97.8% to 104.1%. Consequently, this work provides a portable and effective method for assessing AA levels in actual urine samples.

Keywords: visual detection; ascorbic acid; radical TTM-DMODPA; non-catalytic; smartphone camera

check for updates

Received: 24 June 2025
Revised: 19 July 2025
Accepted: 25 July 2025
Published: 27 July 2025

Citation: Zhong, Q.; Zong, H.; Xie, X.; Rong, X.; Yan, C. Radical TTM-DMODPA for Ascorbic Acid Non-Catalytic Visual Detection. *Chemosensors* **2025**, *13*, 277. https://doi.org/10.3390/chemosensors13080277

Copyright: © 2025 by the authors. Licensee MDPI, Basel, Switzerland. This article is an open access article distributed under the terms and conditions of the Creative Commons Attribution (CC BY) license (https://creativecommons.org/licenses/by/4.0/).

1. Introduction

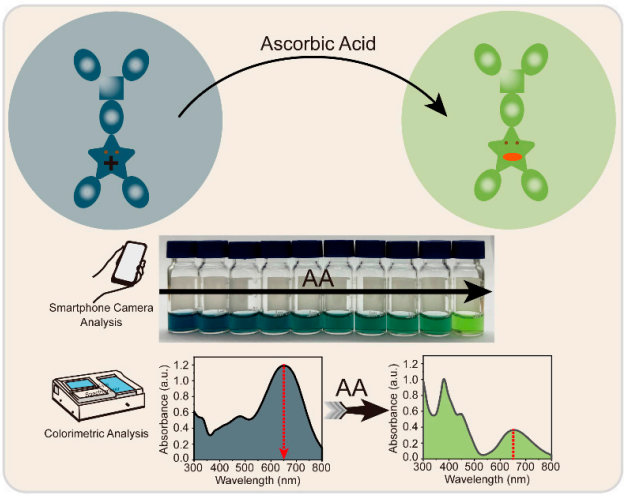
Ascorbic acid (AA) exerts multidimensional roles in human physiological and pathological processes [1–3]. Its core functions primarily involve maintaining redox homeostasis, modulating immune regulation, and facilitating tissue repair [4–6]. Physiologically, ascorbic acid plays an important role in antioxidant defense, collagen synthesis, immune regulation, and iron metabolism regulation [7–10]. In the pathological process, AA is indispensable for combating infectious diseases, chronic diseases, inflammation, and allergy [11–15]. AA functions as a pivotal nexus between nutritional metabolism and disease defense through maintaining redox homeostasis, promoting collagen formation, and enhancing immunity through a triple mechanism. Its deficiency or excess can disrupt physiological balance and precipitate pathological manifestations [16–21]. Therefore, monitoring AA concentrations in biological fluids constitutes a critical diagnostic imperative.

There are many methods for detecting AA, including electrochemical [22], chromatographic [23], enzymatic [24–26], chemiluminescence [27], UV-vis [28,29], and fluorescence

spectroscopic analysis [30,31]. The detection of ascorbic acid holds significant clinical and nutritional importance, as it serves as a key biomarker for oxidative stress assessment and dietary supplementation monitoring [32,33]. While conventional techniques offer valuable detection capabilities, certain practical considerations warrant attention. Electrochemical approaches may be susceptible to electrode surface contamination, chromatographic analysis requires advanced instruments, enzymatic systems can demonstrate variable stability profiles, and fluorescence-based detection frequently requires extensive sample preparation [34]. These challenges motivate the development of simpler yet robust detection platforms. Among these, the colorimetric method has emerged as the preferred routine detection modality owing to its operational simplicity, cost-effectiveness, and high throughput, especially in resource-limited scenarios [35–37]. To date, most colorimetric detection methods for AA predominantly rely on the TMB colorimetric reaction, which requires the participation of enzymes or mimic enzymes [35,37,38], making the composition of the detection system complex. These observations indicate that enzyme-dependent systems may face challenges in achieving optimal performance for colorimetric detection. Some primary constraints should be addressed regarding potential instability in field applications and the existing challenges for point-of-care diagnostics within biological matrices. Therefore, the expansion of colorimetric detection materials and the development of more simplified detection systems for AA are desirable for the efficient and multi-scene detection of AA. Particularly, enzyme-free systems could bridge this gap by combining the simplicity of colorimetry with environmental adaptability.

Organic neutral radicals containing unpaired electrons are a type of natural redox stimuli-responsive material [39]. Owing to the high activity of the intramolecular unpaired electrons, organic radicals exhibit responsive behavior toward electric fields and chemical redox species [40]. Among various reported organic radicals, tris (2,4,6-trichlorophenyl)methyl (TTM) radicals have garnered significant interest owing to their excellent light/thermal stability, adjustable optical properties, and naked-eye-detectable redox responsiveness [41–43]. Consequently, it is accessible to realize the colorimetric detection for redox species using TTM-based radical materials. Notably, no prior studies have demonstrated non-catalytic visual AA detection mediated by organic radical systems.

In this work, a novel organic neutral radical, 4,4′-dimethoxydiphenylamine-substituted tris(2,4,6-trichlorophenyl)methyl (radical TTM-DMODPA), was designed and synthesized. The recovery of radical from its TTM-DMODPA cation was observed with AA injecting, accompanied by characteristic absorbance attenuation and the change in absorption profiles as well as colorimetric transition from blue to grass green (Scheme 1).



Scheme 1. Illustration for ascorbic acid visual detection.

Based on this, a linear relationship between AA concentrations and absorbance variation was found with the help of a UV-vis spectrophotometer. Furthermore, smartphone-based RGB analysis demonstrated comparable linearity, validating the on-site detection capability. In summary, we have developed a non-catalytic convenient visual analysis method for AA detection based on radical TTM-DMODPA and applied it in actual urine samples, which provided a fresh perspective for the material and approach development of biological detection and diagnosis.

2. Materials and Methods

2.1. Chemicals and Reagents

Hydrochloric acid (HCl), hydrogen peroxide (H_2O_2), chloroform, and toluene were procured from Sinopharm Chemical Reagent Co., Ltd. (Shanghai, China). 1,3,5-trichlorobenzene, aluminum chloride ($AlCl_3$), 4,4′-dimethoxydiphenylamine, tetrahydrofuran (THF) potassium tert-butoxide (*t*-BuOK), and *p*-chloranil were ordered from Anhui Senrise Technology Co., Ltd. (Heifei, China). bis(dibenzylideneacetone)palladium ($Pd(dba)_2$), 2,2-bis(diphenylphosphino)-1,1-binaphthalene (BINAP), and sodium tert-butoxide (*t*-BuONa) were purchased from Shanghai Titan Technology Co., Ltd. (Shanghai, China). Ascorbic acid (AA), potassium chloride (KCl), sodium chloride (NaCl), calcium chloride ($CaCl_2$), glucose, glycine (Gly), methionine (Met), uric acid, urea, and cysteine (Cys) were purchased from Adamas Reagents Co., Ltd. (Shanghai, China). All commercially available reagents have not been further purified.

2.2. Equipment and Characterization

^{1}H NMR (500 MHz) and ^{13}C NMR (125 MHz) spectra were measured on a Bruker Avance III HD spectrometer. Signal multiplicities are abbreviated as s (singlet), d (doublet), m (multiplet). High-resolution mass spectroscopies (HRMS) were collected using a Thermal Orbitrap Exploris 120 mass spectrometer. Electron paramagnetic resonance (EPR) spectra of radicals were obtained on a Bruker EMXPlus at ambient temperature. UV-vis absorption spectra were recorded using a 754PC UV-vis spectrophotometer (Yixin Scientific Instrument, Shanghai, China) with 1 nm resolution.

2.3. Synthesis of Compound HTTM-DMODPA

Compound HTTM was prepared following the literature procedures [44].

Under nitrogen atmosphere, a mixture of compound HTTM (1.30 g, 2.35 mmol), 4,4′-dimethoxydiphenylamine (0.32 g, 1.41 mmol), $Pd(dba)_2$ (0.14 g, 0.24 mmol), BINAP (0.16 g, 0.26 mmol), *t*-BuONa (0.68 g, 7.05 mmol), and anhydrous toluene (30 mL). The mixture was refluxed at 105 °C for 14 h. After cooling to room temperature, the solvent was removed under vacuum, and the crude product was purified by silica gel column chromatography (DCM/PE = 1:7 *v*/*v*). White solid HTTM-DMODPA was obtained in 44% yield (0.46 g).

2.4. Synthesis of Radical TTM-DMODPA

Under nitrogen atmosphere, a mixture of compound HTTM-DMODPA (0.12 g, 0.16 mmol), *t*-BuOK (0.72 g, 6.40 mmol), and dry THF (10 mL) was stirred for 40 h at room temperature in the absence of light. Then the *p*-chloranil (0.79 g, 3.20 mmol) was added, and the solution was stirred for another 24 h. The solvent was removed under vacuum, and the crude product was purified by silica gel column chromatography (DCM/PE = 1:9 *v*/*v*). Dark green solid TTM-DMODPA was obtained in 55% yield (0.07 g).

2.5. Procedures for Ascorbic Acid Assay

After mixing 40 μL of radical TTM-DMODPA (760 μM), 10 μL of H_2O_2 (12 mM), and 10 μL of HCl (8 mM), 300 μL of acetonitrile was added and incubated at 60°C for 5 min to obtain the TTM-DMODPA cation. Then 40 μL of ascorbic acid with different concentrations was added to obtain a series of test solutions. After reaction at room temperature for 1 min, their UV-vis spectra and images were recorded. The absorbance change at 652 nm was defined as ΔA ($\Delta A = A_0 - A$, where A and A_0 represent the absorbance of the detection system with and without ascorbic acid, respectively), which was used as the dependent variable of the standard curve to optimize the detection conditions. Triplicate measurements were performed for all experimental conditions.

3. Results and Discussion

3.1. Synthesis and Characterization of Radical TTM-DMODPA

The target radical TTM-DMODPA (Figure 1A) was prepared through sequential dehydrogenation and oxidative transformation of its precursor HTTM-DMODPA, itself synthesized via C-N cross-coupling of HTTM with 4,4′-dimethoxydiphenylamine (Scheme S1, Figure 1A). The ^{1}H and ^{13}C NMR spectra confirmed the successful synthesis of radical precursor HTTM-DMODPA (Figures S1 and S2). HRMS analysis of radical TTM-DMODPA showed the consistent peak position of 745.8936 (m/z) with the calculation value of 745.8943 (Figures 1B and S3), confirming the radical's molecular formula. EPR spectroscopy (Figure 1C) revealed g = 2.003, demonstrating the open-shell radical structure with unpaired electrons and corroborating literature reports [45]. As depicted in Figure 1D, TTM-DMODPA showed an intense absorption peak around 381 nm corresponding to the π−π* transitions of the TTM congeneric family, and the whole absorption profile was also consistent with those reported triarylmethyl radicals [46].

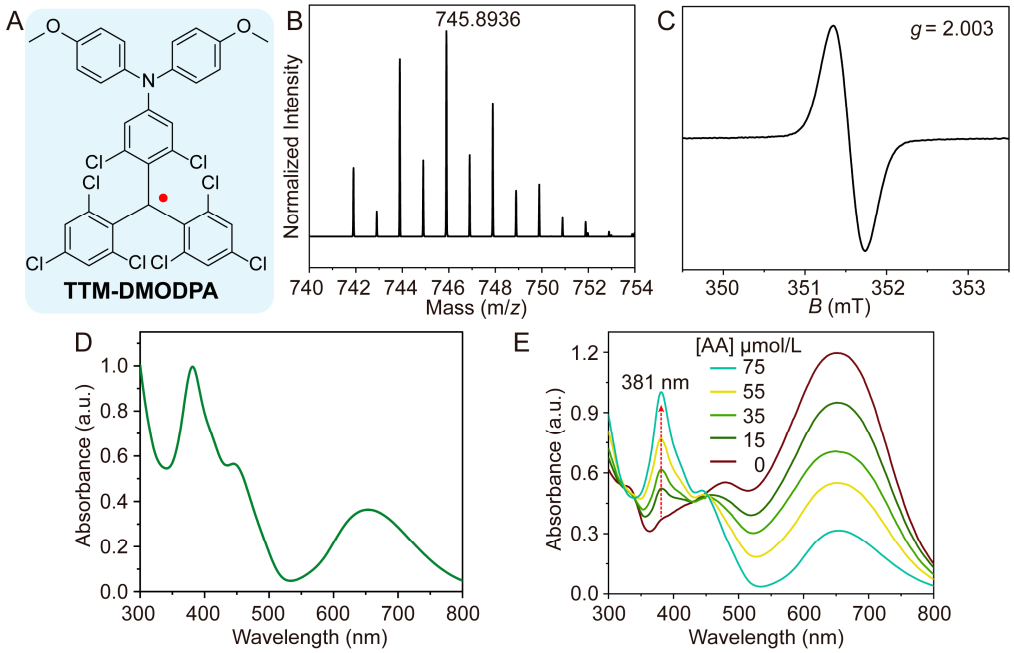


Figure 1. TTM-DMODPA: (**A**) molecular structure, (**B**) high resolution mass spectra (HRMS), (**C**) electron paramagnetic resonance (EPR), (**D**) UV-vis absorption spectrum, and (**E**) UV-vis absorption spectra of TTM-DMODPA cation with the addition of AA (0, 15, 35, 55, 75 μmol/L) within the range of 300–800 nm. The red dot is used as a conventional marker for radical and belongs to the category of universal symbols.

3.2. Feasibility Analysis

Primary investigation of AA-mediated regeneration of the quinoidal TTM-DMODPA cation [44] revealed significant spectral changes. As shown in Figure 1E, it was found that with the addition of AA, the absorbance value of the radical characteristic absorption peak at 381 nm gradually recovered from 0.370 to 1.009. As shown in Figure 2A, TTM-DMODPA cation with quinoid structure is a typical electron-deficient species [47]. Upon the addition of AA, the positively charged nitrogen center atom would first be reduced to the corresponding neutral state, accompanied by the generation of dehydroascorbic acid (DHAA), and then the intramolecular electronic isomerization would occur to afford a stable aromatic sextet structure and the recovery of the radical structure. With the recovery of radical TTM-DMODPA, the absorption profiles of the systems would change significantly, which also provided the accessibility for specific detection of AA [48]. In the visible region, the maximum absorption peak is located at 652 nm. The injection of AA lead to the falling off of its absorbance value from 1.195 to 0.316 at 652 nm. The absorbance value decreased by 3.78 times, as shown in Figure 2B. The color has changed from blue to grass green. These mean that the addition of AA will restore the oxidized cations to their radical form. As shown in Figure 2C, the Benesi–Hildebrand (B–H) technique was employed to determine the binding stoichiometry of the TTM-DMODPA cation and ascorbic acid, and 1:1 binding stoichiometry was obtained by plotting $1/(A_0 - A)$ versus $1/[AA]$ [49,50]. Taken together, these results indicated that the UV-vis spectra and color changes in TTM-DMODPA cation have the potential to detect AA.

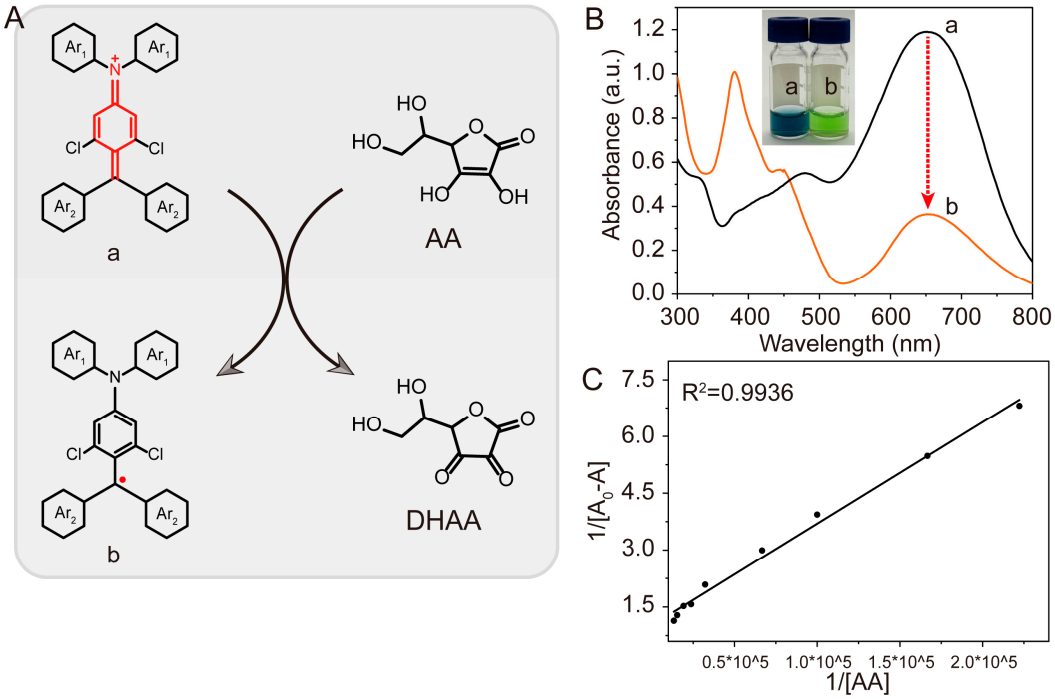


Figure 2. (**A**) Reaction diagram of AA with TTM-DMODPA cation (Red: quinoid structure). (**B**) The UV-vis absorption spectra of different systems. Insert: the corresponding photograph. (a: TTM-DMODPA/H_2O_2. b: TTM-DMODPA/H_2O_2/AA) (**C**) B-H plot of TTM-DMODPA cation and AA.

3.3. Colorimetric Detection of Ascorbic Acid

Based on the above results, we next attempt to optimize and validate the TTM-DMODPA cation recovery assay with the addition of AA. To maximize sensitivity, a systematic study was conducted on the incubation and reaction time, incubation and reac-

tion temperature, as well as the concentration of HCl and H_2O_2 in the reaction system to identify optimal experimental conditions for sensing strategies. We firstly optimized the incubation and reaction time (Figure 3A). Radical TTM-DMODPA, H_2O_2, and HCl were mixed under 60 °C to investigate incubation time. As the incubation time increases, Δ*A* gradually increases from 0 to 5 min and then stabilizes after 5 min. This profile confirmed 5 min as the optimal incubation duration, ensuring complete cation generation without over-oxidation. AA was added to TTM-DMODPA cation solution to investigate reaction time, and it showed a sharp enhancement within 1 min, suggesting the rapid radical recovery reaction caused by AA. The effect of incubation and reaction temperature was also verified. As shown in Figure 3B, the incubation Δ*A* increased between 20 to 60 °C and remained constant. The reaction Δ*A* remained stable after 30 °C. Therefore, incubation temperature of 60 °C and reaction temperature of room temperature were employed for further experiments. The concentration of H_2O_2 and HCl will greatly affect the intensity of the colorimetric signal, so it also needs to be optimized. By comparing the Δ*A* of different HCl concentrations, it is found that as the concentration increases from 0 to 200 μmol/L, the Δ*A* of TTM-DMODPA cation at 652 nm gradually increases and then tends to flat (Figure 3C). Thus, 200 μmol/L of HCl was selected as the suitable concentration for subsequent experiments. The concentration of H_2O_2 affects the degree to which radical TTM-DMODPA forms cations. As the concentration of H_2O_2 increases, it shows an increasing trend below 300 μmol/L and then gradually decreases slightly. Consequently, 300 μmol/L H_2O_2 was identified as the compromise point.

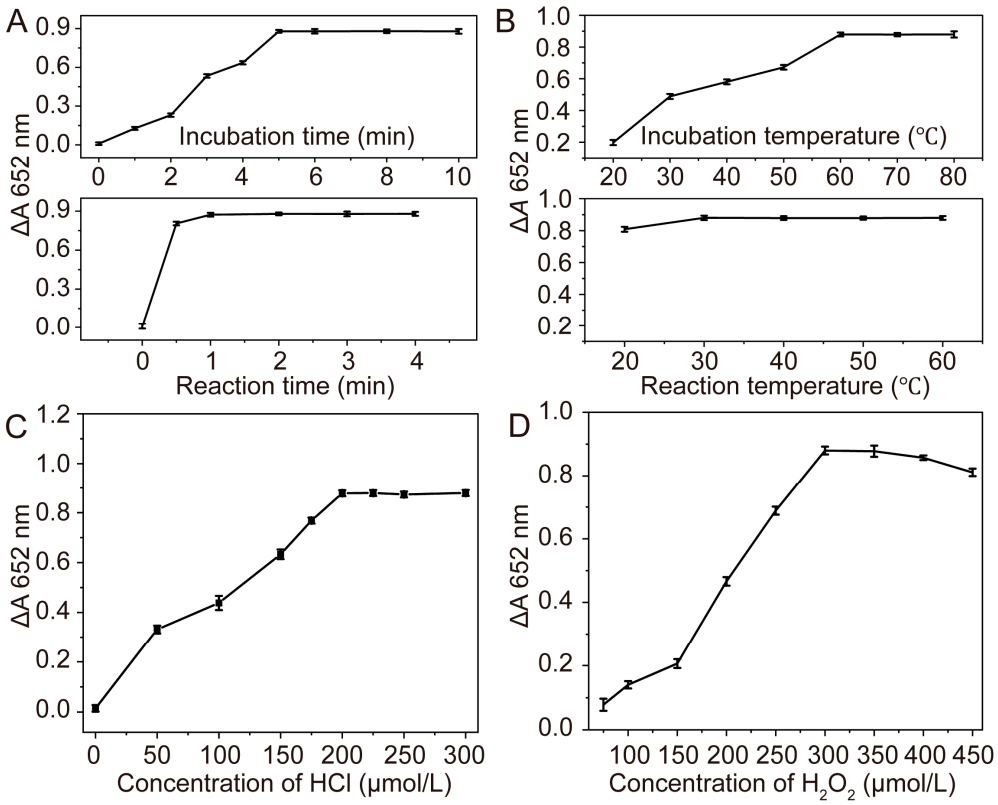


Figure 3. The optimizations of experimental conditions. Effect of (**A**) incubation and reaction time, (**B**) incubation and reaction temperature, (**C**) concentration of HCl, and (**D**) concentration of H_2O_2 on the absorbance change at 652 nm.

Supported by optimizing experimental conditions, the reproducibility, the linear response range, detection limit, and selectivity of the method were evaluated. The TTM-DMODPA cation showed a relatively small relative standard deviation (RSD ≤ 4.50%)

after interacting with multiple concentrations of AA (Figure 4), confirming robust method reproducibility under variable analyte loads.

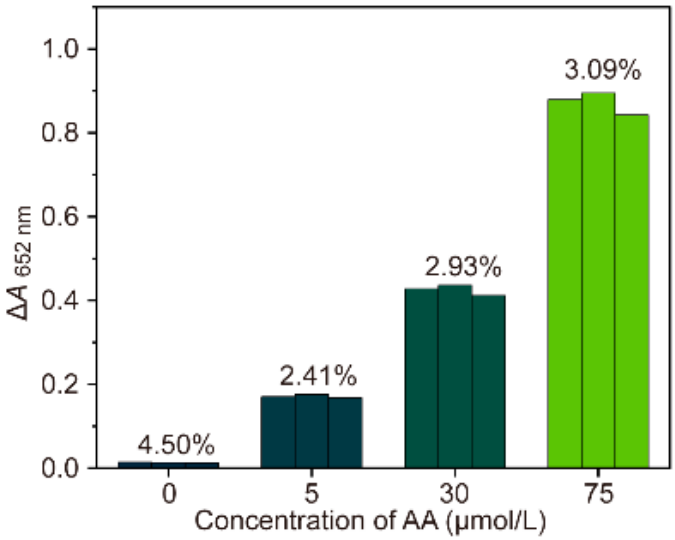


Figure 4. Histogram of Δ*A* intensity with the concentration of AA = 0, 5, 30, 75 μmol/L.

As shown in Figure 5A, the absorbance gradually decreases with increasing AA concentration. Consequently, the absorbance change value at 652 nm ($\Delta A_{652\ nm}$) was used for quantitative analysis of AA. As shown in Figure 5B, there is a good linear relationship between the concentrations of $\Delta A_{652\ nm}$ and AA in the range of 1.25~75 μmol/L. The regression analysis of the data resulted in the following equation: $\Delta A_{652\ nm} = 0.0104C_{AA} + 0.1068$ ($R^2 = 0.9984$). Based on the 3σ/slope (σ is the standard deviation of 15 blank solution measurements), the detection limit (LOD) was calculated as 0.288 μmol/L. As shown in Table 1, compared with other recently reported methods for AA spectral detection techniques, this work using TTM-DMODPA cation as probe exhibits better or comparable analytical performance in the linear range or LOD. Notably, this method is not applicable to any heavy metals, precious metals, or catalysts. And it only requires radical TTM-DMODPA, H_2O_2, and HCl. The composition of the reaction system is simple and easy to control. All of these indicate that TTM-DMODPA cation is an ideal probe for detecting AA concentration in UV-vis spectroscopy.

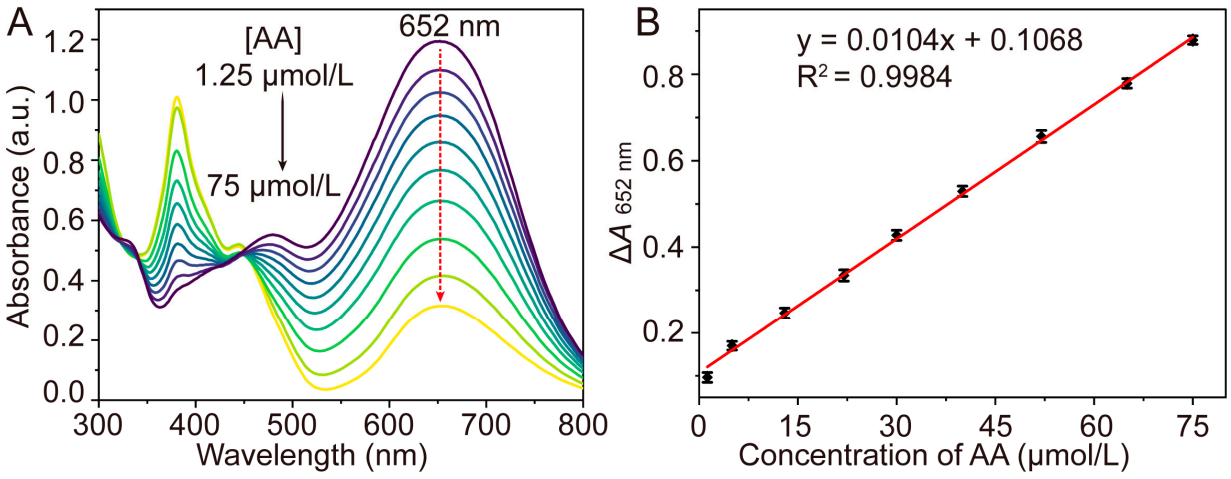


Figure 5. (**A**) UV-vis absorption spectra in the presence of various AA concentrations. (**B**) The linear relationship between $\Delta A_{652\ nm}$ and AA concentration.

Table 1. Comparison of the present work for AA detection with recently reported methods.

Detection System	Analytical Method	Linear Range (μM)	LOD (μM)	References
Fe-CuO + TMB	colorimetric	5–50	4.66	[51]
Fe-N-C + TMB	colorimetric	0.1–2	0.1	[52]
N-GQDs/Fe_3O_4@Co_9S_8 + TMB	colorimetric	1–70	0.404	[53]
$CuMnO_2$ + TMB	colorimetric	1–105	0.39	[54]
CoOOH-ABTS	colorimetric	0.5–15	0.16	[55]
SiQDs + MnO_2	fluorometric	1–80	0.48	[56]
Au@MnO_2	fluorometric	0.75–17.5	0.47	[57]
Ti_3C_2QDs + CoOOH	fluorometric	0–100	0.19	[58]
CdTe QDs	fluorometric	10–250	1.3	[59]
Eu MOF	fluorometric	0–3.0	0.32	[60]
TTM-DMODPA cation	colorimetric	1.25–75	0.288	This work

Considering the importance of anti-interference performance in actual sample detection, 16 interfering substances (K^+, Na^+, Mg^{2+}, Ca^{2+}, Cl^-, glucose, Gly, Met, uric acid urea, Cys, citric acid, tartaric acid, and lactic acid) were employed to evaluate the selectivity for TTM-DMODPA cation toward AA determination. As demonstrated in Figure 6, with the exception of AA, none of the interfering substances exhibited significant $\Delta A_{652\ nm}$ values. Therefore, the TTM-DMODPA cation demonstrates excellent specificity for AA determination in complex matrices.

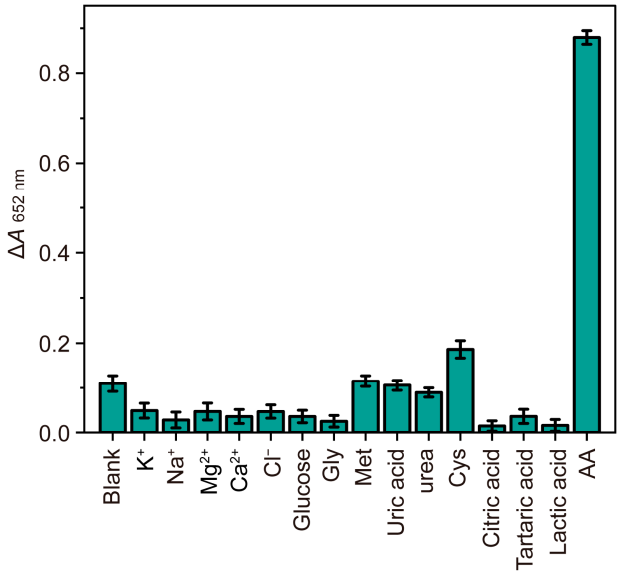


Figure 6. The selectivity of TTM-DMODPA cation system to AA (AA is 75 μmol/L, and other substances are 500 μmol/L).

3.4. Camera Photography Analysis

To validate the field applicability of the colorimetric method, smartphone-captured images of reaction solutions containing graded AA concentrations were systematically analyzed (Figure 7A), with subsequent RGB value extraction demonstrating linear correlation (R^2 = 0.9910) with AA concentration, thereby confirming the reliability of this instrument-free visual detection platform for on-site quantitative analysis. The RGB values are then quantitatively analyzed using the Euclidean distance (EDs = $(\Delta R^2 + \Delta G^2 + \Delta B^2)^{1/2}$). The quantitative analysis results are shown in Figure 7B. The linear relationship between EDs and AA concentration ranges from 0~65 μmol/L. The LOD was determined to be

1.46 µmol/L. Therefore, the proposed method demonstrates superior analytical performance for AA analysis and provides an instrument-free visual detection strategy.

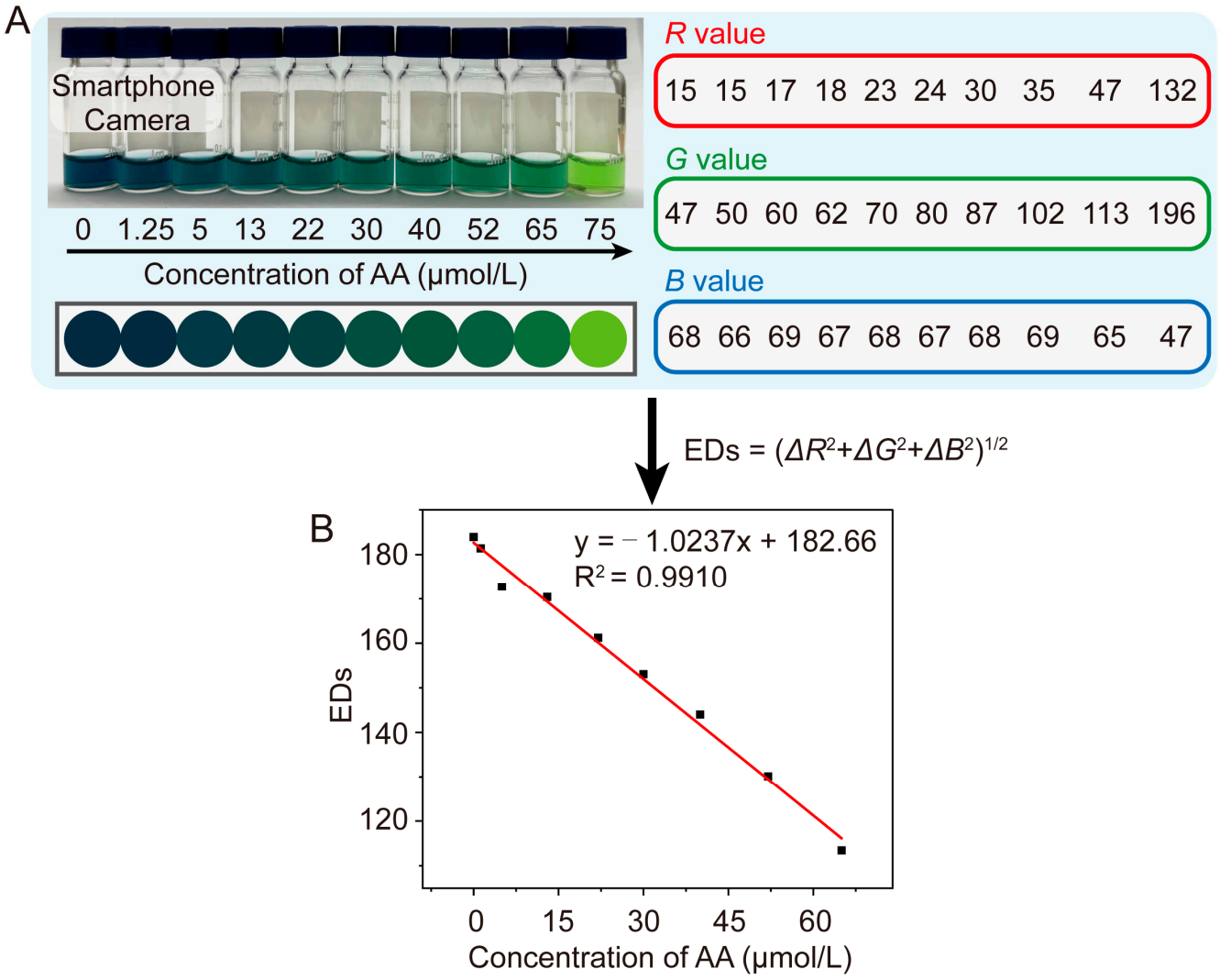


Figure 7. Analysis based on smartphone camera: (**A**) colorimetric picture taken by smartphone camera and the corresponding RGB values. (**B**) The linear relationship between ED value and added AA concentration.

3.5. Urine Sample Detection

As explained before, the proposed TTM-DMODPA cation system demonstrated excellent linearity and selectivity for AA quantification, rendering it particularly suitable for detecting the concentration in actual samples. The detection of AA content in urine can be used to evaluate vitamin C intake, identify interference factors in urine tests, and assist in the diagnosis of metabolic or kidney diseases in specific situations. To verify the usability of the TTM-DMODPA cation system, AA detection was performed in urine samples provided by adult volunteers in our team. Then, the standard addition method was used for spiked recovery experiments to check the accuracy of our system (Table 2). The concentrations of AA in urine were found to be 121.5 and 93.8 µmol/L, respectively. The recovery of AA in urine samples of healthy volunteers was between 97.8% and 104.1%, and the relative standard deviation (RSD, n = 3) at each concentration was less than 4.03%. All these acceptable results declare the potential application of AA detection in actual urine samples.

Table 2. Measurements of AA in human urine samples.

Samples [1]	Added (μM)	Found (μM)	Recovery (%)	RSD (n = 3, %)
Urine 1	0.0	12.15	–	2.69
	5.0	17.27	102.4	4.03
	10.0	22.09	99.4	3.88
Urine 2	0.0	9.38	–	3.28
	5.0	14.27	97.8	1.12
	10.0	19.79	104.1	2.32

[1] The urine samples were diluted 10 times for detection.

4. Conclusions

In summary, we have synthesized a novel radical TTM-DMODPA and established a new colorimetric detection method by utilizing the property of AA to restore its oxidation state to radical. Under the reaction conditions of incubation time of 5 min, temperature of 60 °C, H_2O_2 concentration of 300 μmol/L, and HCl concentration of 200 μmol/L, it has analytical performance comparable to the methods reported in the literature. And successfully applied in human urine samples with satisfactory AA recovery. The constructed smartphone camera system is suitable for on-site analysis scenarios without analytical instruments. It also provides a portable and effective method to perform AA analysis in actual samples. This provides a convenient and innovative approach for biological detection and diagnosis. Despite the limitation in in situ monitoring capabilities, this instrument-free approach represents a significant advancement toward portable AA quantification in resource-limited settings, offering new possibilities for decentralized healthcare diagnostics.

Supplementary Materials: The following supporting information can be downloaded at: https://www.mdpi.com/article/10.3390/chemosensors13080277/s1, Scheme S1: Synthetic Route for radical TTM-DMODPA; Figures S1-S2: ^{1}H and ^{13}C NMR spectra of new compounds; Figure S3: HRMS spectrum (ESI) of radical TTM-DMODPA.

Author Contributions: Conceptualization, C.Y.; methodology, C.Y.; validation, Q.Z., H.Z., and X.X.; formal analysis and investigation, Q.Z. and X.R.; resources, C.Y.; data curation, C.Y.; writing—original draft preparation, Q.Z.; writing—review and editing, C.Y. and Q.Z.; supervision, C.Y. All authors have read and agreed to the published version of the manuscript.

Funding: This research was funded by the National Natural Science Foundation of China (No. 22304048), the Natural Science Foundation of Hunan Province (No. 2023JJ40096), the Scientific Research Project of Hengyang Normal University (No. 2024QD07, No. 2022QD05), and the Foundation of Hunan Engineering Research Center for Monitoring and Treatment of Heavy Metals Pollution in the Upper Reaches of Xiangjiang River (No. 2023HSKFJJ014).

Institutional Review Board Statement: Ethical review and approval were waived for this study because the urine samples collected from laboratory staff were fully anonymized and did not involve any personal identifiers or sensitive health information.

Informed Consent Statement: Informed consent was obtained from all subjects involved in the study.

Data Availability Statement: Data are available upon reasonable request from the authors.

Conflicts of Interest: The authors declare no conflicts of interest.

References

1. Zheng, Z.; Liu, L.; Ouyang, S.; Chen, Y.; Lin, P.; Chen, H.; You, Y.; Zhao, P.; Huang, K.; Tao, J. In Situ Ratiometric Determination of Cerebral Ascorbic Acid after Ischemia Reperfusion. *ACS Sens.* **2023**, *8*, 4587–4596. [CrossRef]
2. Zeng, Z.; Wang, J.; Zhao, S.; Zhang, Y.; Fan, J.; Wu, H.; Chen, J.; Zhang, Z.; Meng, Z.; Yang, L.; et al. A Bioinspired Flexible Sensor for Electrochemical Probing of Dynamic Redox Disequilibrium in Cancer Cells. *Adv. Sci.* **2023**, *10*, 2304079. [CrossRef]

3. He, X.; Wang, Q.; Cheng, X.; Wang, W.; Li, Y.; Nan, Y.; Wu, J.; Xiu, B.; Jiang, T.; Bergholz, J.S.; et al. Lysine Vitcylation Is a Vitamin C-derived Protein Modification That Enhances STAT1-mediated Immune Response. *Cell* **2025**, *188*, 1858–1877.e1821. [CrossRef]
4. Yi, Z.; Yang, X.; Liang, Y.; Tong, S. Iron Oxide Nanozymes Enhanced by Ascorbic Acid for Macrophage-based Cancer Therapy. *Nanoscale* **2024**, *16*, 14330–14338. [CrossRef]
5. Qian, Y.; Gao, Y.; Wang, D.; Zhang, S.; Luo, Q.; Shan, G.; Lu, M.; Yan, D.; Tang, B.Z.; Zhang, M. A Tactfully Designed Photothermal Agent Collaborating with Ascorbic Acid for Boosting Maxillofacial Wound Healing. *Natl. Sci. Rev.* **2025**, *12*, nwae426. [CrossRef]
6. Jaber, M.; Jaber, B.; Hamed, S.; AlKhatib, H.S. Preparation and Evaluation of Ascorbyl Glucoside and Ascorbic Acid Solid in Oil Nanodispersions for Corneal Epithelial WoundHealing. *Int. J. Pharm.* **2022**, *627*, 122227. [CrossRef]
7. Favarin, F.R.; Forrati, É.M.; Bassoto, V.A.; da Silva Gündel, S.; Velho, M.C.; Ledur, C.M.; Verdi, C.M.; Lemos, J.G.; Sagrillo, M.R.; Fagan, S.B.; et al. Ascorbic Acid and Ascorbyl Palmitate-loaded Liposomes: Development, Characterization, Stability Evaluation, in Vitro Security Profile, Antimicrobial and Antioxidant Activities. *Food Chem.* **2024**, *460*, 140569. [CrossRef]
8. Meacham, C.E.; DeVilbiss, A.W.; Morrison, S.J. Metabolic Regulation of Somatic Stem Cells in Vivo. *Nat. Rev. Mol. Cell Biol.* **2022**, *23*, 428–443. [CrossRef]
9. Schoenfeld, J.D.; Sibenaller, Z.A.; Mapuskar, K.A.; Wagner, B.A.; Cramer-Morales, K.L.; Furqan, M.; Sandhu, S.; Carlisle, T.L.; Smith, M.C.; Abu Hejleh, T.; et al. O_2- and H_2O_2-Mediated Disruption of Fe Metabolism Causes the Differential Susceptibility of NSCLC and GBM Cancer Cells to Pharmacological Ascorbate. *Cancer Cell* **2017**, *31*, 487–500.e488. [CrossRef]
10. Wang, H.; You, Q.; Kang, B.; Jing, H.; Shi, Z.; Krizkova, S.; Heger, Z.; Adam, V.; Chen, X.; Li, N. Pulling the Rug Out from Under: Biomechanical Microenvironment Remodeling for Induction of Hepatic Stellate Cell Quiescence. *Adv. Mater.* **2024**, *36*, 2406590. [CrossRef]
11. Leesang, T.; Yap, Y.S.; Brabson, J.P.; Klimas, A.; Ahearn, E.L.; Barbieri, D.A.; Lam, M.Q.; Lyon, P.D.; Figueroa, M.K.E.; Beckedorff, F.; et al. Retinoic Acid and Ascorbate Remodel the Epigenome of Leukemia Cells to Improve Therapeutic Efficacy By Enhancing TET Activity. *Blood* **2023**, *142*, 5706. [CrossRef]
12. Fu, D.; Liu, H.; Chen, T.; Cheng, Y.; Cao, M.; Liu, J. A Bio-analytic Nanoplatform Based on Au Post-functionalized $CeFeO_3$ for The Simultaneous Determination of Melatonin and Ascorbic Acid through Photo-assisted Electrochemical technology. *Biosens. Bioelectron.* **2022**, *213*, 114457. [CrossRef]
13. Liang, X.-H.; Yu, A.-X.; Bo, X.-J.; Du, D.-Y.; Su, Z.-M. Metal/Covalent-organic Frameworks-based Electrochemical Sensors for The Detection of Ascorbic Acid, Dopamine and Uric acid. *Coord. Chem. Rev.* **2023**, *497*, 215427. [CrossRef]
14. Yang, X.; Lin, X.; Li, J.; Viitala, T.; Zhao, Y.; Zhang, H.; Shang, L. Vitamin C Encapsulated Biomimetic Nanogels with Macrophage Membrane Decoration for Chronic Wound Healing. *Chem. Eng. J.* **2025**, *505*, 159080. [CrossRef]
15. Koga, T.; Kawahara, N.; Aburada, M.; Ono, A.; Mae, S.; Yoshida, A.; Iwaoka, Y.; Ito, H.; Tai, A. Antiallergic Activity of 3-O-Dodecyl-l-ascorbic Acid. *Molecules* **2024**, *29*, 69. [CrossRef]
16. Wang, M.; He, J.; Li, S.; Cai, Q.; Zhang, K.; She, J. Structural Basis of Vitamin C Recognition and Transport by Mammalian SVCT1 Transporter. *Nat. Commun.* **2023**, *14*, 1361. [CrossRef]
17. Pouptsis, A.; Zaragoza, R.; Garcia-Trevijano, E.R.; Vina, J.R.; Ortiz-Zapater, E. Nutrition, Lifestyle, and Environmental Factors in Lung Homeostasis and Respiratory Health. *Nutrients* **2025**, *17*, 954. [CrossRef]
18. Costa, M.G.; da Silva, B.C.; Alves, D.M.R.; de Lima, P.S.R.; Prado, R.d.M. Silicon, by modulating homeostasis and nutritional efficiency, increases the antioxidant action and tolerance of bell peppers to phosphorus deficiency. *Sci. Hortic.* **2025**, *343*, 114093. [CrossRef]
19. Zhang, S.; Wang, N.; Gao, Z.; Gao, J.; Wang, X.; Xie, H.; Wang, C.-Y.; Zhang, S. Reductive stress: The key pathway in metabolic disorders induced by overnutrition. *J. Adv. Res.* **2025**. [CrossRef]
20. Sato, A.; Kondo, Y.; Ishigami, A. The evidence to date: Implications of l-ascorbic acid in the pathophysiology of aging. *J. Physiol. Sci.* **2024**, *74*, 29. [CrossRef]
21. Edzeamey, F.J.; Ramchunder, Z.; Gomez, A.V.; Ge, H.; Marobbio, C.M.T.; Pourzand, C.; Virmouni, S.A. Therapeutic combination of L-ascorbic acid, N-acetylcysteine, and dimethyl fumarate in Friedreich's ataxia: Insights from in vitro models. *Redox Rep.* **2025**, *30*, 2505303. [CrossRef]
22. Kumar, R.; Shafique, M.S.; Chapa, S.O.M.; Madou, M.J. Recent Advances in MOF-Based Materials for Biosensing Applications. *Sensors* **2025**, *25*, 2473. [CrossRef]
23. Galal, S.A.B.; Elzanfaly, E.S.; Hussien, E.M.; Amer, E.A.H.; Zaazaa, H.E. Sustainable Thin-Layer Chromatographic Method for the Determination of Ipriflavone and Vitamins in Bone Health Supplements. *J. Anal. Chem.* **2025**, *80*, 480–489. [CrossRef]
24. Yildiz, G.; Yildiz, G. Insights into Ultrasound-Assisted Postharvest Preservation: Metabolic, Structural, and Quality Changes in Strawberries During Storage. *Food Bioprocess Technol.* **2025**. [CrossRef]
25. Ma, J.; Zou, M.; Peijnenburg, W.; Chen, F. Priming agents combat copper stress in wheat (*Triticum aestivum* L.) under hydroponic conditions: Insights in impacts on morpho–physio–biochemical traits and health risk assessment. *Ecotoxicol. Environ. Saf.* **2025**, *291*, 117899. [CrossRef]

26. Lv, J.; Chen, S.; Xu, W.; Zhang, X.; Wang, M.; Xu, J.; Zhu, Z.; Hu, Q.; Niu, L. Lectin-Mediated Labeling of Alkaline Phosphatase for Enzymatic Silver Deposition-Based Electrochemical Detection of Glycoprotein Tumor Markers. *Anal. Chem.* **2025**, *97*, 2479–2485. [CrossRef]
27. Agar, M.; Laabei, M.; Leese, H.S.; Estrela, P. Multi-Template Molecularly Imprinted Polymeric Electrochemical Biosensors. *Chemosensors* **2025**, *13*, 11. [CrossRef]
28. Zhang, X.; Zhou, X.; Wan, Q.; Sun, T.; Gao, G. A smartphone sensing colorimetric detection of ascorbic acid in fruit samples based on $Cu_2Fe(CN)_6$@PVP nanozyme. *Talanta* **2025**, *293*, 128125. [CrossRef]
29. Rocha, F.R.P.; Zagatto, E.A.G. Chemical Derivatization in Flow Analysis. *Molecules* **2022**, *27*, 1563. [CrossRef]
30. Wu, N.; Liu, W.; Yang, S.; Wang, G.; Zhang, Z.; Guo, S. Construction of ratio fluorescence sensor based on fluorescence scattering characteristics and its analytical application. *Microchem. J.* **2025**, *213*, 113829. [CrossRef]
31. Gao, Y.; Wang, J.; Mu, X.; Liu, B.; Xia, M.; Wang, F.; Tong, Z. Carbon quantum dots in spectrofluorimetric analysis: A comprehensive review of synthesis, mechanisms and multifunctional applications. *Talanta* **2025**, *293*, 128066. [CrossRef]
32. Zhu, Q.; Dong, D.; Zheng, X.; Song, H.; Zhao, X.; Chen, H.; Chen, X. Chemiluminescence determination of ascorbic acid using graphene oxide@copper-based metal–organic frameworks as a catalyst. *RSC Adv.* **2016**, *6*, 25047–25055. [CrossRef]
33. Dalapati, R.; Biswas, S. Aqueous Phase Sensing of Fe^{3+} and Ascorbic Acid by a Metal–Organic Framework and Its Implication in the Construction of Multiple Logic Gates. *Chem. Asian J.* **2019**, *14*, 2822–2830. [CrossRef]
34. Zhang, W.; Li, X.; Liu, X.; Song, K.; Wang, H.; Wang, J.; Li, R.; Liu, S.; Peng, Z. A Novel Electrochemical Sensor Based on Pd Confined Mesoporous Carbon Hollow Nanospheres for the Sensitive Detection of Ascorbic Acid, Dopamine, and Uric Acid. *Molecules* **2024**, *29*, 2427. [CrossRef]
35. Zhou, H.; Luo, H.; Tong, Y.; Zhuang, Q.-F.; Wang, Y. Colorimetric Detection of Ascorbic Acid Based on Oxidase-like Activity of Fe_2O_3/Nitrogen-doped Carbon Nanomaterials. *Chin. J. Anal. Chem.* **2025**, *53*, 346–355. [CrossRef]
36. Sang, Y.; Wu, P.; Ge, J.; Cao, Y.; Xiao, Y.; Yang, Y.; Wang, C.; Li, Z.; Cai, R. Bimetallic CuAg nanoflowers with high nanozyme activity for detection of acid phosphatase. *Microchem. J.* **2025**, *213*, 113808. [CrossRef]
37. Qi, J.; Tian, L.; Pang, Y.; Wu, F. Manganese Phthalocyanine-Based Magnetic Core-Shell Composites with Peroxidase Mimetic Activity for Colorimetric Detection of Ascorbic Acid and Glutathione. *Molecules* **2025**, *30*, 1484. [CrossRef]
38. Kukreja, E.A.; Tripathi, R.M.; Chung, S.J. Colorimetric and smartphone-based dual modality sensing platform for detection of ascorbic acid. *Sens. Actuators A* **2025**, *389*, 116573. [CrossRef]
39. Pu, Z.; Xu, Z.; Zhang, X.; Guo, Y.; Sun, Z. Unlocking the Multistage Redox Property of Graphenic Radicals by π-Extension. *Angew. Chem. Int. Ed.* **2024**, *63*, e202406078. [CrossRef]
40. Kodama, T.; Aoba, M.; Hirao, Y.; Rivero, S.M.; Casado, J.; Kubo, T. Molecular and Spin Structures of a Through-Space Conjugated Triradical System. *Angew. Chem. Int. Ed.* **2022**, *61*, e202200688. [CrossRef]
41. Chen, L.; Arnold, M.; Kittel, Y.; Blinder, R.; Jelezko, F.; Kuehne, A.J.C. 2,7-Substituted N-Carbazole Donors on Tris(2,4,6-trichlorophenyl)methyl Radicals with High Quantum Yield. *Adv. Optical Mater.* **2022**, *10*, 2102101. [CrossRef]
42. Matsuda, K.; Xiaotian, R.; Nakamura, K.; Furukori, M.; Hosokai, T.; Anraku, K.; Nakao, K.; Albrecht, K. Photostability of Luminescent Tris(2,4,6-trichlorophenyl)methyl Radical Enhanced by Terminal Modification of Carbazole Donor. *Chem. Commun.* **2022**, *58*, 13443–13446. [CrossRef]
43. Yan, C.; Fang, J.; Zhu, J.; Chen, W.; Wang, M.; Chi, K.; Lu, X.; Zhou, G.; Liu, Y. Donor Engineering of Diphenylamine-substituted Tris(2,4,6-trichlorophenyl)methyl Radicals for Controlling the Intramolecular Charge Transfer and Near-infrared Photothermal Conversion. *J. Mater. Chem. C* **2023**, *11*, 2729–2736. [CrossRef]
44. Peng, Q.; Obolda, A.; Zhang, M.; Li, F. Organic Light-Emitting Diodes Using a Neutral π Radical as Emitter: The Emission from a Doublet. *Angew. Chem. Int. Ed.* **2015**, *54*, 7091–7095. [CrossRef]
45. Ai, X.; Chen, Y.; Feng, Y.; Li, F. A Stable Room-Temperature Luminescent Biphenylmethyl Radical. *Angew. Chem. Int. Ed.* **2018**, *57*, 2869–2873. [CrossRef]
46. Murto, P.; Li, B.; Fu, Y.; Walker, L.E.; Brown, L.; Bond, A.D.; Zeng, W.; Chowdhury, R.; Cho, H.-H.; Yu, C.P.; et al. Steric Control of Luminescence in Phenyl-Substituted Trityl Radicals. *J. Am. Chem. Soc.* **2024**, *146*, 13133–13141. [CrossRef]
47. Yan, C.; An, D.; Chen, W.; Zhang, N.; Qiao, Y.; Fang, J.; Lu, X.; Zhou, G.; Liu, Y. Stable Diarylamine-Substituted Tris(2,4,6-trichlorophenyl)methyl Radicals: One-Step Synthesis, Near-Infrared Emission, and Redox Chemistry. *CCS Chem.* **2022**, *4*, 3190–3203. [CrossRef]
48. Facure, M.H.M.; Mercante, L.A.; Gogotsi, Y.; Correa, D.S. ZnO–Co_3O_4 Nanofibers/MXene Composite with Peroxidase-Like Activity for Ascorbic Acid Detection. *ACS Appl. Nano Mater.* **2025**, *8*, 4291–4299. [CrossRef]
49. Hebbar, S.D.; Trivedi, D.R. Discriminative ion detection of Hg^{2+} and Cu^{2+} and selective recognition of PO_4^{3-} ions: Real time monitoring in food and water samples and molecular keypad lock integration. *Spectrochim. Acta Part A* **2025**, *331*, 125706. [CrossRef]

50. Mane, P.V.; Patil, P.; Mahishi, A.A.; Kigga, M.; Bhat, M.P.; Lee, K.-H.; Kurkuri, M. Rhodamine 6G derivative for the selective copper detection and remediation using nanoporous diatomaceous earth-engineered functional receptor. *Heliyon* **2023**, *9*, e16600. [CrossRef]
51. Yan, B.; Yang, Y.; Xie, Y.; Li, J.; Li, K. Fe Doping Enhances the Peroxidase-Like Activity of CuO for Ascorbic Acid Sensing. *Chemistry* **2023**, *5*, 1302–1316. [CrossRef]
52. Gu, Y.; Cao, Z.; Zhao, M.; Xu, Y.; Lu, N. Single-Atom Fe Nanozyme with Enhanced Oxidase-like Activity for the Colorimetric Detection of Ascorbic Acid and Glutathione. *Biosensors* **2023**, *13*, 487. [CrossRef]
53. Meng, R.; Li, S.; Li, W.; Wang, Q.; Wang, Y.; Hao, S.; Zhang, D.; Zhou, X. Highly dispersed Co_9S_8 loaded on Fe_3O_4 modified by graphene quantum dots for ascorbic acid detection. *Microchem. J.* **2025**, *212*, 113411. [CrossRef]
54. Lian, Q.; Zheng, X.; Peng, G.; Liu, Z.; Chen, L.; Wu, S. Oxidase mimicking of $CuMnO_2$ nanoflowers and the application in colorimetric detection of ascorbic acid. *Colloids Surf. A* **2022**, *652*, 129887. [CrossRef]
55. Fang, X.; Wang, J.; Cui, X.; Zhang, Y.; Zhu, R.; Zhao, H.; Li, Z. Sensitive and facile colorimetric sensing strategy for ascorbic acid determination based on CoOOH nanoflakes-ABTs oxidative system. *Colloids Surf. A* **2019**, *575*, 66–74. [CrossRef]
56. Ma, F.; Luo, J.; Li, X.; Liu, S.; Yang, M.; Chen, X. A "switch-on" fluorescence assay based on silicon quantum dots for determination of ascorbic acid. *Spectrochim. Acta, Part A* **2021**, *249*, 119343. [CrossRef]
57. Huang, L.; Qin, S.; Yang, K.; Xu, Y.; Wu, X.; Lin, Z.; Wang, Y. Dual signal AA detection based on fluorescence and local surface plasmon resonance absorption technology. *Spectrochim. Acta Part A* **2024**, *306*, 123570. [CrossRef]
58. Hu, F.; Mao, Y.; Huang, J.; Wan, L.; Liu, S.; Wen, Z.; Ai, F. "On–off–on" fluorescent sensor based on Ti_3C_2 quantum dots and CoOOH nanosheets for the detection of ascorbic acid. *New J. Chem.* **2024**, *48*, 5258–5266. [CrossRef]
59. Zhu, J.; Zhao, Z.-J.; Li, J.-J.; Zhao, J.-W. Fluorescent detection of ascorbic acid based on the emission wavelength shift of CdTe quantum dots. *J. Lumin.* **2017**, *192*, 47–55. [CrossRef]
60. Dong, X.-X.; Chen, T.-L.; Kong, X.-J.; Wu, S.; Kong, F.-F.; Xiao, Q. A facile fluorescence Eu MOF sensor for ascorbic acid and ascorbate oxidase detection. *Anal. Methods* **2024**, *16*, 704–708. [CrossRef]

Disclaimer/Publisher's Note: The statements, opinions and data contained in all publications are solely those of the individual author(s) and contributor(s) and not of MDPI and/or the editor(s). MDPI and/or the editor(s) disclaim responsibility for any injury to people or property resulting from any ideas, methods, instructions or products referred to in the content.